NIH Public Access
Author Manuscript
Cancer Res. Author manuscript; available in PMC 2012 September 15.

Published in final edited form as:
Cancer Res. 2012 March 15; 72(6): 1557–1567. doi:10.1158/0008-5472.CAN-11-3596.

Kras^{G12D} and p53 mutation cause primary intra-hepatic cholangiocarcinoma

Michael R. O'Dell[1,*], **Jing-Li Huang**[1,*], **Christa L. Whitney-Miller**[2,*], **Vikram Deshpande**[3], **Paul Rothberg**[2], **Valerie Grose**[1], **Randall M. Rossi**[1], **Andrew X. Zhu**[3], **Hartmut Land**[4], **Nabeel Bardeesy**[3], and **Aram F. Hezel**[1]

[1]James P. Wilmot Cancer Center, University of Rochester School of Medicine, 300 Elmwood Avenue, Rochester, NY 14642, USA

[2]Department of Pathology and Laboratory Medicine University of Rochester School of Medicine, 300 Elmwood Avenue, Rochester, NY 14642, USA

[3]Massachusetts General Hospital, Harvard Medical School, 55 Fruit Street, Boston, Massachusetts 02114, USA

[4]Department of Biomedical Genetics Medicine University of Rochester School of Medicine, 300 Elmwood Avenue, Rochester, NY 14642, USA

Abstract

Intrahepatic cholangiocarcinoma (IHCC) is a primary cancer of the liver with a rising incidence and poor prognosis. Preclinical studies of the etiology and treatment of this disease are hampered by the relatively small number of available IHCC cell lines or genetically faithful animal models. Here we report the development of a genetically engineered mouse model of IHCC that incorporates two of the most common mutations in human IHCC, activating mutations of Kras (Kras^{G12D}) and deletion of p53. Tissue-specific activation of Kras^{G12D} alone resulted in the development of invasive IHCC with low penetrance and long latency. Latency was shortened by combining Kras^{G12D} activation with heterozygous or homozygous deletion of p53 (mean survival of 56 weeks versus 19 weeks, respectively), which also resulted in widespread local and distant metastasis. Serial analysis showed that the murine models closely recapitulated the multistage histopathologic progression of the human disease, including the development of stroma-rich tumors and the pre-malignant biliary lesions, intraductal papillary biliary neoplasms (IPBN) and Von Meyenburg complexes (VMC; also known as biliary hamartomas). These findings establish a new genetically and histopathologically faithful model of IHCC and lend experimental support to the hypothesis that IPBN and VMC are precursors to invasive cancers.

Keywords

biliary tract cancer; Intraductal papillary biliary neoplasm; IPBN; Von Meyenburg complex; autophagy; chloroquine; LC3

Introduction

Intra-hepatic cholangiocarcinoma (IHCC) is thought to arise from the intra-hepatic biliary system based on common histological and molecular properties (1). These tumors are

Corresponding Author: Aram F. Hezel at: Aram_Hezel@URMC.Rochester.edu; phone: 585 273 4150; fax: 585 276 0337. James P. Wilmot Cancer Center, University of Rochester School of Medicine, 300 Elmwood Avenue, Rochester, NY 14642, USA.
*These authors contributed equally to this work.

NIH-PA Author Manuscript
NIH-PA Author Manuscript
NIH-PA Author Manuscript

NIH-PA Author Manuscript

NIH-PA Author Manuscript

NIH-PA Author Manuscript

characterized by an aggressive course and early metastasis. The incidence of IHCC is on the rise and while effective palliative chemotherapy has recently been defined, treatment options for the majority of patients remain limited (2, 3). Many aspects of its biology and genetics remain incompletely defined including key questions relating to 1) the cell(s)-of-origin, 2) the precursor lesions in the liver, their molecular profiles, and their relationship to fully established IHCC and 3) the functional impact of oncogenes and tumor suppressor genes on malignant progression.

While the genetic basis for IHCC has not been fully elucidated, mutations in a number of established oncogenes and tumor suppressors are well described. Recurrent mutations have been observed in the KRAS oncogene, which is activated in 20% to 50% of tumors (4–6). Mutations in BRAF were described in two European cohorts but have not been reported in the US studies (1). p53 inactivation is the most common tumor suppressor lesion, observed in 37% of IHCC (7). Additionally, subsets of IHCC show mutations or deletions of SMAD4 and $p16^{INK4A}$ (4, 8).

Pathologic studies of the biliary system in diseased livers and of biliary lesions adjacent to IHCC have led to a proposed multi-stage progression model for the development of invasive cancers from the normal hepatic epithelium (9). In particular, lesions known as biliary intraepithelial neoplasia (BilIN) and intraductal papillary biliary neoplasms (IPBN) are thought to be precursors of IHCC and have been graded according to the degrees of architectural distortion and cellular atypia (10, 11). Additional lesions of the biliary tract include malformations of the ductal systems referred to as biliary hamartomas or Von Meyenburg complexes, although the relationship of these lesions to IHCC is less clear (12, 13). Importantly, despite these detailed pathologic descriptions, the genetic features of the different biliary ductal lesions and the capacity of these lesions to give rise to IHCC remain undefined.

Experimental model systems have been central to providing basic and preclinical insights into many cancer types. While a number of advances have been made in this regard in IHCC, there is currently an incomplete array of systems for the study of this malignancy. For example, only a small number of IHCC cell lines are reported in the literature, with most published experimental studies employing no more than two or three lines. Alternatively, studies often employ a combination of IHCC, EHCC, and gall bladder cell lines, although these different types of biliary cancer carry distinct mutational profiles. A number of carcinogen-induced models of primary liver tumors in mammalian systems have been described (14–17) and the transduction of viral onco-proteins has also enabled transformation of carcinogen treated hepatic epithelium both in vitro and in vivo (18, 19). Genetically engineered mouse (GEM) models have also been developed to model tumors with similarities to IHCC. p53 mutant mice develop cholangiocarcinomas upon repeated carcinogen exposure, although there is long latency in this model (20). Liver targeted delivery of mouse polyoma virus middle T antigen (PyMT) using a transgenic avian retroviral system induces focal regions of IHCC as well as more prominent hepatocellular carcinoma (HCC) lesions in Trp53 and Ink4a/Arf knockout mice (21). Mixed HCC/IHCC histology is also seen in mice with liver specific inactivation of the NF2, Sav1, and Mst1/Mst2 tumor suppressor genes, although HCC is the predominant component in each case (reviewed in (22)). Combined homozygous deletion of conditional *Smad4* and *Pten* alleles in the liver via crosses to the Albumin-Cre strain causes tumors histologically similar to IHCC (23). While providing important systems to study malignant transformation of liver cells, these models have not been reported to exhibit progressive precursor lesions of the biliary tract nor do they accurately incorporate the most common genetic lesions seen in the human disease.

NIH-PA Author Manuscript

NIH-PA Author Manuscript

NIH-PA Author Manuscript

GEM models designed to mimic both genetic and pathologic aspects of cancer have proven critical to drug development efforts, biomarker identification, and the study of early disease (24, 25). In order to create a model of IHCC based on oncogenic mutations commonly observed in the human disease we generated compound mutant mice with Albumin-Cre mediated somatic activation of $Kras^{G12D}$ and deletion of p53 in the hepatic parenchyma. We report that cooperation between these two relevant genetic alterations in the hepatic epithelium leads to a model of IHCC that recapitulates the histologic and molecular features of multistage progression of human IHCC. We employ this model to study the role of pre-invasive lesions as precursors to IHCC, and use a panel of IHCC-derived cell lines to show that autophagy may be an important targetable pathway in this malignancy as in some other Kras-driven carcinomas. Thus, our work establishes a relevant and faithful preclinical model system with which to study this challenging disease.

Material and Methods

Mice

Mutant mouse strains—All animal studies were conducted in accordance with the AAALAC accredited University Committee on Animal Resources (UCAR). All mouse strains used in these studies have been previously described and characterized (26–28). Specifically $Kras^{G12D}$, $p53^{L/L}$, and Alb-Cre mutants strained were intercrossed to achieve the desired cohorts as outlined above. The genetic background was mixed. Individual mice within experimental cohorts were followed until signs of illness including poor grooming, abdominal bloating, diminished activity or weight loss at which point a full necropsy was performed followed by histological analysis.

Histology

Two board-certified pathologists with a specialization in hepatic histopathology independently reviewed and classified tumors. In all cases there was agreement about the histological diagnosis. Lymph nodes, lungs and spleen were included in a survey for metastasis in all individuals with tumors.

Tumor cell lines

After sampling of tumors for histology and molecular profiling 3–5 mm samples of tumor derived from mutant mouse strains described above were cut adjacent to sample evaluated histologically and subjected to collagenase/trypsin digestion. After washing cells were placed in DMEM with 10% FCS and fed until a confluent monolayer was formed. Cells were passaged 3–4 times prior to molecular characterization that included IF staining with CK-19 to establish ductal origin and repeated genotyping for Kras and p53 to establish hepatic origin.

Immunohistochemistry

Formalin-fixed paraffin sections were hydrated and heat-mediated antigen retrieval was carried out when necessary. Sections were then incubated with primary antibody overnight at 4°C. Species and isotype matched IgG were used in place of the primary antibodies as a negative control.

Western blotting

Whole tissues (liver and whole tumor) were snap frozen in liquid nitrogen crushed immediately using an electronic pestle into ice-cold lysis buffer. Cells used were grown to 60–80% confluence in the presence of fresh complete media rinsed 2X with PBS and scraped off the plate in the presence of ice-cold lysis buffer. Cell Signaling lysis buffer (cat

NIH-PA Author Manuscript

NIH-PA Author Manuscript

NIH-PA Author Manuscript

9803) including Sigma Protease Inhibitor Cocktail (cat# P8340), Sigma Phosphatase Inhibitor Cocktail 2 (cat# P5726), and Sigma Phosphatase Inhibitor Cocktail 3 (cat # P0044) were used for all experiments. Protein concentration was determined using the Bradford assay.

Antibodies

Cell Signalling—GAPDH (14C10) #2118, P-Akt Ser473 #9271, Akt #9272, p44/42 MAPK (Erk1/2) (137F5) #4695, P-p44/42 MAPK (Erk1/2) (Thr202/Tyr204) (D13.14.4E) #4695, p53 (1C12) #2524, LC3A (D50G8) #4599. Santa Cruz: alpha-Tubulin (TU-02) sc-8035, p21 (H-164) sc-756, p16 (M-156) sc-1207, Smad4 (B-8) sc-7966, Cytokeratin 19 (M-17): sc-33111. Abcam: p19ARF ab80. Progen: p62. Dako: pan-CK #Z0622 1:1000., AFP (#A0008) 1:400.

Autophagy assays

Culture conditions; cells were grown in DMEM with 10% FBS, L-glutamine, no antibiotics and media was changed every 1–2 days or the morning prior to analysis. pBabe-LC3-GFP (Addgene, 11546) was used to produce virus using NIH3T3 cells. Standard infection protocol with polybrene was followed to establish low-passage cell explants with the GFP-LC3 autophagy reporter. To determine GFP-LC3 foci counts cells were plated onto cover slips in the presence and absence of Chloroquine at the indicated dosage, and fixed with 4% paraformaldehyde. Confocal images were taken with FV1000 Olympus laser scanning microscope. At least 50 cells were counted for each cell line under different treatment conditions. Cells containing more than 5 puncta were considered positive for autophagy. For the cell proliferation assays, cells were seeded in 24-well plates at 10,000 cells per well. Treatment with Chloroquine at the indicated dose was performed the day after plating. At the indicated time points, cells were fixed with 10% formalin and stained with 0.1% crystal violet. Dye was extracted with 10% acetic acid and OD at 595nm was determined as a measure of relative cell density.

Statistical analysis

All statistical analysis was performed using Prism statistical software version 4.0a May 11, 2003. Survival was determined using the Kaplan-Meir method and comparisons between treatment groups were determined using the Log-rank test. Animals that displayed signs of illness and were found to have advanced cancers on necropsy were included as events as were all animals that died prior to developing signs of illness that had a liver mass identified at autopsy. Animals that died for reasons other than advanced cancer, as determined by the absences of liver pathology on autopsy were censored.

Results

Mutations in Kras and p53 are among the most commonly described genetic changes in IHCC. In order to model these genetic features in the mouse we used a conditionally activated allele for $Kras^{G12D}$ (LSL-$Kras^{G12D}$) and a conditional knockout allele for p53 ($p53^{Lox)}$ (26, 27). The LSL-$Kras^{G12D}$ allele is expressed at endogenous levels after Cre-mediated excision of a transcriptional stopper element and the $p53^{Lox}$ allele is engineered to sustain Cre-mediated excision of exons 2–10 rendering the gene functionally inactive. While the cell of origin of IHCC is not established, both the differentiated biliary epithelial cells as well as resident progenitor cells within the liver, commonly referred to as "oval cells," have been implicated (29). Further complicating the understanding of the ontogeny of IHCC is the finding that human IHCC harbors regions of abnormal intermediate hepatocytes and that HCC expresses markers typically seen in IHCC (30). Given the undefined cellular origins of these tumors we sought an approach that would target mutations throughout the adult liver.

NIH-PA Author Manuscript

NIH-PA Author Manuscript

NIH-PA Author Manuscript

To accomplish this, we used the Albumin-Cre (Alb-Cre) transgene which is initially active in liver progenitors during late embryogenesis and has been shown to produce effective recombination of floxed alleles in both the adult hepatocytes and cholangiocytes (Fig. 1A) (28). Cohorts of compound mutant mice were created with the experimental genotypes Alb-Cre;$Kras^{G12D}$ (n=8), Alb-Cre;$Kras^{G12D}$;$p53^{L/L}$ (n=20), and Alb-Cre;$Kras^{G12D}$;$p53^{L/+}$(n=22) — from here on designated Kras, Kras-$p53^{L/+}$, and Kras-$p53^{L/L}$ mice, respectively.

$Kras^{G12D}$ cooperates with p53 inactivation to cause hepatic transformation

Kras, Kras-$p53^{L/+}$, and Kras-$p53^{L/L}$ cohorts were produced at the expected ratios and showed no evidence of early developmental abnormalities. These animals were monitored until they developed signs of illness (abdominal bloating, diminished activity and cachexia). Most of the Kras mice were healthy up to an age of 75 weeks, although 1 of 8 developed a lethal liver mass at 36 weeks of age. p53 deficiency greatly increased the penetrance and accelerated disease onset as the Kras-$p53^{L/+}$ and Kras-$p53^{L/L}$ mice developed tumors as early as 32 and 9 weeks, respectively (mean survival 52 weeks and 19 weeks; Fig. 1B). Upon necropsy these animals were found to have solid liver tumors ranging in size from 2 mm to 20 mm and presented as isolated nodules (n=14 mice) or as multiple independent lesions (n=6 mice) (Table 1). In many animals, cystic fluid filled lesions were found adjacent to the solid masses (Fig 1C). Hepatic lesions frequently demonstrated hemorrhage into the peritoneal cavity and had evidence of tumor necrosis. Tumors were highly metastatic, with 75% of tumor bearing animals displaying gross evidence of invasion into adjacent organs (diaphragm, bowel, pancreas and stomach) or distant metastasis (with dissemination to the lymph nodes, spleen, lungs, and peritoneal cavity) (Fig 2B and Table 1). Mice harboring Alb-Cre;$p53^{L/L}$ (n=10) were followed to 1 year of age without evidence of illness, and subsequent necropsy and histological survey did not reveal abnormal hepatic pathology (data not shown). Thus, $Kras^{G12D}$ promotes metastatic liver tumorigenesis that is significantly accelerated by the heterozygous and homozygous inactivation of p53.

Albumin-Cre; Kras GEM models recapitulate the histopathologic features of human IHCC

Microscopic analysis of the liver tumors revealed that 83% showed IHCC histology, with 66% (n=19) containing exclusively IHCC and 17% (n=5) showing a mixed phenotype of IHCC and hepatocellular carcinoma (HCC) elements. A smaller number had exclusively HCC histology (17% n=5)(Table 1, and Fig. 2A). The IHCC showed a range cellular differentiation, including well-differentiated tumors with clear glandular architecture and areas of mucin production, as well as poorly differentiated tumors with minimal gland formation and large pleomorphic cells demonstrating nuclear atypia and frequent mitosis (Fig. 2A). Often different grades of differentiation were seen in the same tumor. The histologic spectrum of IHCC was similar among the different mouse cohorts.

To further characterize the tumors, we stained tissue sections for cytokeratins (pan-CK) that mark the biliary epithelium and have been used clinically to distinguish IHCC from HCC. Correspondingly, immunochemistry for pan-CK revealed robust staining of the regions with the biliary ductal morphology, consistent with IHCC histopathology (Fig. 2C). In mixed tumors, the areas of glandular epithelium stained positive for pan-CK (Fig. 2Aiii arrow-head and Fig. 2C arrowhead) whereas the regions morphologically consistent with HCC were pan-CK negative (Fig. 2Aiii arrow). We also stained tissue sections for alpha-fetoprotein (AFP) a marker of HCC. Immunochemistry for AFP showed staining of all HCC and HCC components of mixed tumors while IHCC and IHCC components of mixed tumors did not stain (Fig. 2Ciii). Early metastasis is a hallmark of human IHCC and similarly microscopic IHCC metastases were found in nearly all animals examined, including those without evident gross metastasis. These lesions were found in the lung, lymphatic system and the spleen, peritoneal cavity, and veins (Fig. 2B). Trichrome staining revealed collagen

NIH-PA Author Manuscript

NIH-PA Author Manuscript

NIH-PA Author Manuscript

deposition throughout the IHCC but not in most HCC, a pattern reminiscent of the corresponding human tumors, where IHCC, but not HCC, are characterized by a dense stroma (desmoplasia)(Fig 2D). Overall, the histopathological appearance of the murine IHCC displayed a striking similarity to the human disease, exhibiting varying degrees of differentiation and early metastasis.

IHCC is associated with IPBN and Von Meyenburg complexes, or biliary hamartomas

Histological survey of hepatic parenchyma adjacent to IHCC, as well as isolated regions of grossly normal liver, revealed the presence of pre-malignant lesions within the bile ducts. These lesions resembled intraductal papillary neoplasms of the bile ducts (IPBN) and biliary hamartomas (also known as von Meyenburg complexes, VMC) that have been described in humans (11, 12). In several cases, there was evidence that the IHCC arose directly from IPBN (Fig. 1C and Fig. 3B). The presence of additional lesions in regions distal to the primary tumors suggests that there was multifocal initiation of these precursor lesions. IPBN were grossly evident (Fig 1Cii- lower cystic lesion with arrowhead), characterized by dilated bile ducts (Fig. 3Ai & iii), and were found were connected to the biliary tree. These structures were lined by pancreaticobiliary and intestinal epithelium, and exhibited varying degrees of dysplasia, with a notable frequent association of the largest lesions with contiguous areas of invasive carcinoma (Fig3B). While a papillary architecture was not universally appreciated the presence of low-grade dysplasia in some areas and high-grade dysplasia/carcinoma in situ in others mimicked the typical presentation seen in the human disease (Fig 3Ai–iv). These observations support the IPBN-to-IHCC progression model for this cancer type.

In addition to the IPBN, another type structural abnormality was seen in focal regions of the biliary ducts, consisting of dilated, haphazardly arranged ductal structures embedded in a fibrous stroma adjacent to portal areas. Such structures, found in found in 36% of animals harboring IHCC (n=5/14) (Fig 4i–v), showed resemblance to biliary hamartomas or Von Meyenburg complexes (VMC) described in humans. While these lesions were typically small and focused, in two animals we also observed more extensive lesions that extended through an entire lobe of the liver (Fig. 4Aii). Whereas VMC are generally been regarded as benign, recent case reports of cholangiocarcinoma arising from a VMC have raised the question of its potential role as an IHCC precursor lesion (12, 31). Consistent with this notion, we found IHCC apparently arising directly from adjacent VMC in four animals (Fig. 4iii). VMC showed strong staining for pan-CK consistent with their ductal morphology (Fig. 4Aii and 4Bii). The findings of both IPBN and VMC, both independent of and in association with IHCC, among mutant Kras-p53 animals provides experimental evidence for a progression model of IHCC that includes both IPBN as well as VMC.

Molecular features of IHCC

In order to characterize the molecular features of IHCC arising in the Kras-p53 mice we used both early passage cell lines derived from the primary tumors and whole tumor lysates. Tumor cells were used to evaluate other established tumor suppressor genes (TSG) and provide a pure tumor-derived material without stromal contamination. CK-19, a common marker of IHCC, confirmed the origins of early passage tumor explants with all derivative cells demonstrating positive immunostaining (data not shown). As expected p53 and its downstream target, p21, were not expressed in the IHCC (Fig. 5A) consistent with somatic deletion (data not shown). Among tumors arising in Kras-p53 $^{L/+}$ mice we found loss of the wild-type allele in 4/6 animals consistent with spontaneous deletion during the course of tumorigenesis (Fig. 5B). Next, we examined Smad4 and p16^{Ink4a}, which are additional tumor suppressors known to be inactivated in human IHCC (4, 32, 33). Western blot analysis showed that Smad4 expression was maintained in all six IHCC examined, whereas

NIH-PA Author Manuscript

NIH-PA Author Manuscript

NIH-PA Author Manuscript

$p16^{Ink4a}$ expression was absent in two lines (#335 and 460). The $p19^{Arf}$ tumor suppressor, expressed from a common locus with $p16^{Ink4a}$ was also absent in line #335, suggesting somatic deletion of the Ink4a/Arf (CDKN2A) locus. All other lines retained various levels of $p19^{Arf}$ expression in these p53 deficient tumors, consistent with the overlapping functions of p53 and $p19^{Arf}$ in constraining tumor progression (34). The spontaneous loss of wild-type p53 in tumors arising in the Kras-$p53^{L/+}$ cohort and the sporadic loss of $p16^{Ink4a}$ mirrors the molecular profile of the human disease and is in keeping with key functions of the p53/$p19^{Arf}$ and Rb/$p16^{INK4A}$ pathways in suppressing KRAS-driven tumorigenesis.

Next we performed a molecular analysis of IHCC to determine the status of pathways that are commonly altered in human IHCC. Whole IHCC lysates were compared with both normal liver as well as with normal appearing liver from Kras-p53 animals. Both MAPK/MEK and PI3K/AKT/mTOR signaling pathways have been shown to be active and important for growth and survival in tumors characterized by KRAS mutation and strategies to target these downstream effectors of KRAS are in development in IHCC (35, 36). Consistent with KRAS activation and signaling through MAPK/MEK signaling pathways we found total ERK1/2 levels to be elevated in tumors compared to both normal liver as well as liver harboring concurrent Kras/p53 mutations (Fig 5C), that latter of which exhibited no increased activity of the pathway despite the presence of a Kras mutation in the majority of cells. Phosphorylation of residues Thr 202 and Tyr 204 indicative of Erk1/2 activity was present in IHCC but not found in the untransformed hepatic epithelium (Fig 5C). Similarly PI3K/AKT pathway activity was seen as evidenced by phosphorylation of AKT Ser 473 in IHCC. Enhanced expression and activation of components of both MAPK/MEK and PI3K pathways is consistent with the observations made among human tumors as well as with other tumors driven by KRAS and points towards the potential utility of inhibitors under development targeting these pathways.

IHCC are characterized by elevated levels of autophagy required for growth

The panel of cell lines from our GEM model provides a genetically defined experimental system to begin to test the role of key pathways in the pathogenesis of the KRAS-p53 mutant subset of IHCC. Notably, tumors driven by mutated RAS have been difficult to target as compared with cancers which harbor more "druggable" mutated or amplified oncogenes (37). Combinational approaches focused on key downstream pathways, such as combined PI3K and MEK inhibition as discussed above, may offer strategies towards effective treatments. At the same time insights into the unique metabolic requirements of RAS driven tumors and in particular a dependence on autophagy have also led to new therapeutic inroads (38–40). Autophagy (or macro-autophagy) is the process of auto-digestion (or "self-eating") that both maintains cellular homeostasis and enables cells to meet basic energy requirements in times of stress. The induction of autophagy has been proposed to play a dual role in cancer, functioning to suppress cancer progression at the earliest steps- possibly though protection from genomic damage, while allowing advanced cancers to meet their metabolic demands (41). Preclinical evidence suggests therapeutic utility in targeting autophagy in RAS driven tumors prompting us to determine if autophagy is active in the Kras-p53 IHCC model (38). We first evaluated total levels of the microtubule associated protein 1 light chain 3 (LC3), a marker of autophagy that associates with the autophagosome membrane after processing. Total levels of LC3 (including both LC3-I as well as the autophagosome associated lipidated form LC3-II) were elevated in tumors compared with normal and Kras-p53 mutant liver (Fig. 5B, lower band). Among early passage cell lines derived from IHCC grown in nutrient rich conditions we observed high levels of LC3-II as compared with LC3-1, also indicative of active autophagy (Fig. 6A) (42). To more directly evaluate the integration of LC3 into autophagosomes we infected early passage cell lines derived from Kras-p53 IHCC with a GFP-LC3 reporter that has served as

NIH-PA Author Manuscript

NIH-PA Author Manuscript

NIH-PA Author Manuscript

a standard measure of autophagy (42). These cells showed a high incidence GFP-LC3 puncta despite growth under nutrient rich conditions, suggesting that they may exhibit activated autophagy (Fig. 6A). However, since autophagy is a dynamic process, total levels of LC3-I and -II as well as the accumulation of GFP-LC3 puncta could also reflect a defect in the later processing of the autophagosome rather than increased rates of autophagy. Thus, we evaluated the flux through the pathway by blocking the downstream processing of autophagosomes with chloroquine (CQ), which prevents lysosomal acidification and subsequent autophagosome degradation. We found that CQ increased the number of puncta in all four IHCC cell lines tested, confirmed that these cell lines have activated autophagy under basal conditions (Fig. 6B) (42). We next sought to test whether CQ-mediated inhibition of autophagy impairs the proliferation of IHCC cells. Notably, we found that CQ treatment inhibited the growth of four separate early passage cell lines representing both well and poorly differentiated IHCC (Fig. 6C). CQ caused the expected induction of LC3-II across all four lines and increased p62 expression in three of four lines (Fig. 6D). Together these results show that autophagy is actively engaged in Kras-p53 IHCC cells, and that its inhibition using CQ attenuates cell proliferation, thus this approach may have value in the treatment of IHCC.

Discussion

We have generated a GEM model in which KRAS activation combined with p53 inactivation results in the reproducible development of IHCC that mimics the human disease on a pathologic and molecular level. Importantly, the tumors in this model arise from the malignant progression of precursor lesions in the bile ducts, enabling us to provide novel insight into histopathogenesis of the disease, showing in particular that both IPBN and VMC can give rise to IHCC. In terms of the molecular features, the tumors in this model show spontaneous loss of $p16^{Ink4a}$ and show activation of the MAPK/MEK and PI3K/AKT pathways, recapitulating observations from the human cancer. This model provides a relevant foundation for further understanding the earliest precancerous stages of IHCC, the influence of additional genetic lesions on tumor biology, and for evaluating therapeutics.

While IHCC was the dominant histological tumor type we also found a small proportion of mixed IHCC/HCC and HCC. Mixed IHCC/HCC are well recognized clinically and, while sharing some histological characteristics with HCC, behave more similarly to IHCC in terms of the rapidity of disease progression, elevation of tumor markers, and responsiveness to chemotherapy (43). The relationships between dominant histological phenotype (HCC vs. IHCC), molecular underpinning, and clinical behavior of primary liver tumors are not straightforward (30). Recent expression analysis of primary tumors including HCC, IHCC and mixed tumors revealed a subset with a histological diagnosis of HCC but an IHCC-like expression profile which correlated with a more aggressive clinical course (44). Thus, a molecular overlap exists among the human primary liver tumors, despite clear histological differences among subtypes. The development of the mixed tumors and occasional evidence of HCC may reflect the timing of Alb-Cre-mediated recombination that is first evident during late embryogenesis, and thus targets hepatic progenitors and mature hepatocytes, as well as biliary tract epithelium. Kras mutations are found in rare subsets of HCC induced by mutagen exposure, and associated with p53 mutations in this setting (45). Since the entire liver was targeted for mutation and since biliary epithelial cells are only a small proportion of the liver parenchyma, it is notable the dominant phenotype was biliary cancer. This suggests either that biliary cells have particularly susceptibility to Kras transformation or that Kras and p53 mutations shift cellular differentiation toward a biliary phenotype. Future studies using promoters to target Cre expression to subpopulations of cells within the liver (biliary, hepatocyte, or other intermediaries) could clarify this issue.

NIH-PA Author Manuscript

NIH-PA Author Manuscript

NIH-PA Author Manuscript

Both IPBN and Von Meyenburg complexes were found as isolated lesions as well as in association with IHCC in our GEM model. IPBN are an established precursor to human IHCC, whereas the relationship of VMC to malignant tumors in humans has not been defined. VMCs are found in ~5% of adults in autopsy series and are associated with hepatic cysts (13). More recently reports of VMC showing progressive cytological atypia in association with IHCC have raised the question of their importance in a progression model of the disease (12). In our model, we found instances of clear histological progression of IPBN, as well as VMC, to contiguous IHCC, thereby providing direct evidence that both of these precursors can be initiated by KRAS and can progress to invasive cancer. There was no overlap in regions harboring IPBN and VMC, suggesting that there arise independently of each other. It is also notable that a group of tumor-bearing animals showed no evidence for such structures or of any other precursor lesions. One possible explanation for both the independent ontogeny of the IPBN and VMC, and the absence of such lesions in some mice may be that each scenario is associated with a different cell of origin. For example, Kras-p53 mediated transformation of early liver progenitors (hepatoblasts), adult progenitors (e.g. oval cells), and more mature forms of the biliary epithelium or hepatocytes may be associated with a different cellular differentiation program during early tumorigenesis. Alternatively, such differences in precursor lesions may reflect the differential impact of additional acquired molecular alterations driving IHCC progression, as has been reported in pancreatic cancer GEM models (46).

Autophagy is active in derivative cell lines and blockade of autophagy with chloroquine (CQ) inhibits growth of derivative cell lines consistent with findings in other Kras driven tumors (38, 39). While most RAS driven cancer cell lines have evidence of active autophagy the effect of blocking this process has variable effects on cell proliferation, with certain tumor types- including pancreatic cancer- exhibiting marked sensitivity to CQ, while growth of lung cancer cell lines was effected to a lesser extent. We find that cell lines from our model are significantly growth inhibited with a corresponding block in autophagy by CQ. This fits well with evidence from human tumors and cell lines suggesting the importance of autophagy in the human disease and provides impetus to further evaluate CQ and other drugs that may impact this process in IHCC (47, 48).

In summary, we have created a tractable IHCC GEM model based on the genetics of the human disease. The multistage evolution of the tumors provides a context to explore questions regarding the role of different cells of origin and the molecular and histological progression of precancerous stages of IHCC. Additionally, the highly reproducible development of IHCC in this model provides a foundation for testing the influence of additional genetic lesions on tumor biology and a platform for the pre-clinical testing of promising new therapies.

Acknowledgments

We would like to thanks Catherine Harmer for contributing to the organization and preparation of the manuscript and Alec Kimmelman for critical reading of the manuscript. AFH is supported by a HHMI early career award and the Edelman-Gardner foundation award. N.B. is supported by grants from TargetCancer Foundation, and from the NIH (1R01CA136567-01A1). This work is also supported by the Granara-Skerry Trust and was accomplished in the Translational Research Core Facility of the Wilmot Cancer Center at the University of Rochester Medical Center.

References

1. Hezel AF, Deshpande V, Zhu AX. Genetics of biliary tract cancers and emerging targeted therapies. J Clin Oncol. 2011; 28:3531–40. [PubMed: 20547994]

NIH-PA Author Manuscript

NIH-PA Author Manuscript

NIH-PA Author Manuscript

2. Shaib Y, El-Serag HB. The epidemiology of cholangiocarcinoma. Semin Liver Dis. 2004; 24:115–25. [PubMed: 15192785]
3. Valle J, Wasan H, Palmer DH, et al. Cisplatin plus gemcitabine versus gemcitabine for biliary tract cancer. N Engl J Med. 2011; 362:1273–81. [PubMed: 20375404]
4. Tannapfel A, Benicke M, Katalinic A, et al. Frequency of p16(INK4A) alterations and K-ras mutations in intrahepatic cholangiocarcinoma of the liver. Gut. 2000; 47:721–7. [PubMed: 11034592]
5. Tannapfel A, Sommerer F, Benicke M, et al. Mutations of the BRAF gene in cholangiocarcinoma but not in hepatocellular carcinoma. Gut. 2003; 52:706–12. [PubMed: 12692057]
6. Deshpande V, Nduaguba A, Zimmerman SM, et al. Mutational profiling reveals PIK3CA mutations in gallbladder carcinoma. BMC Cancer. 2011; 11:60. [PubMed: 21303542]
7. Tannapfel A, Weinans L, Geissler F, et al. Mutations of p53 tumor suppressor gene, apoptosis, and proliferation in intrahepatic cholangiocellular carcinoma of the liver. Dig Dis Sci. 2000; 45:317–24. [PubMed: 10711445]
8. Argani P, Shaukat A, Kaushal M, et al. Differing rates of loss of DPC4 expression and of p53 overexpression among carcinomas of the proximal and distal bile ducts. Cancer. 2001; 91:1332–41. [PubMed: 11283934]
9. Wu TT, Levy M, Correa AM, Rosen CB, Abraham SC. Biliary intraepithelial neoplasia in patients without chronic biliary disease: analysis of liver explants with alcoholic cirrhosis, hepatitis C infection, and noncirrhotic liver diseases. Cancer. 2009; 115:4564–75. [PubMed: 19670455]
10. Zen Y, Fujii T, Itatsu K, et al. Biliary papillary tumors share pathological features with intraductal papillary mucinous neoplasm of the pancreas. Hepatology. 2006; 44:1333–43. [PubMed: 17058219]
11. Zen Y, Adsay NV, Bardadin K, et al. Biliary intraepithelial neoplasia: an international interobserver agreement study and proposal for diagnostic criteria. Mod Pathol. 2007; 20:701–9. [PubMed: 17431410]
12. Xu AM, Xian ZH, Zhang SH, Chen XF. Intrahepatic cholangiocarcinoma arising in multiple bile duct hamartomas: report of two cases and review of the literature. Eur J Gastroenterol Hepatol. 2009; 21:580–4. [PubMed: 19282767]
13. Redston MS, Wanless IR. The hepatic von Meyenburg complex: prevalence and association with hepatic and renal cysts among 2843 autopsies [corrected]. Mod Pathol. 1996; 9:233–7. [PubMed: 8685220]
14. Kiguchi K, Carbajal S, Chan K, et al. Constitutive expression of ErbB-2 in gallbladder epithelium results in development of adenocarcinoma. Cancer Res. 2001; 61:6971–6. [PubMed: 11585718]
15. Elmore LW, Sirica AE. Phenotypic characterization of metaplastic intestinal glands and ductular hepatocytes in cholangiofibrotic lesions rapidly induced in the caudate liver lobe of rats treated with furan. Cancer Res. 1991; 51:5752–9. [PubMed: 1655260]
16. Lai GH, Zhang Z, Shen XN, et al. erbB-2/neu transformed rat cholangiocytes recapitulate key cellular and molecular features of human bile duct cancer. Gastroenterology. 2005; 129:2047–57. [PubMed: 16344070]
17. Sirica AE, Zhang Z, Lai GH, et al. A novel "patient-like" model of cholangiocarcinoma progression based on bile duct inoculation of tumorigenic rat cholangiocyte cell lines. Hepatology. 2008; 47:1178–90. [PubMed: 18081149]
18. Braun L, Goyette M, Yaswen P, Thompson NL, Fausto N. Growth in culture and tumorigenicity after transfection with the ras oncogene of liver epithelial cells from carcinogen-treated rats. Cancer Res. 1987; 47:4116–24. [PubMed: 2440558]
19. Lin YZ, Brunt EM, Bowling W, et al. Ras-transduced diethylnitrosamine-treated hepatocytes develop into cancers of mixed phenotype in vivo. Cancer Res. 1995; 55:5242–50. [PubMed: 7585583]
20. Farazi PA, Zeisberg M, Glickman J, Zhang Y, Kalluri R, DePinho RA. Chronic bile duct injury associated with fibrotic matrix microenvironment provokes cholangiocarcinoma in p53-deficient mice. Cancer Res. 2006; 66:6622–7. [PubMed: 16818635]

NIH-PA Author Manuscript

NIH-PA Author Manuscript

NIH-PA Author Manuscript

21. Chen YW, Klimstra DS, Mongeau ME, Tatem JL, Boyartchuk V, Lewis BC. Loss of p53 and Ink4a/Arf cooperate in a cell autonomous fashion to induce metastasis of hepatocellular carcinoma cells. Cancer Res. 2007; 67:7589–96. [PubMed: 17699762]
22. Avruch J, Zhou D, Fitamant J, Bardeesy N. Mst1/2 signalling to Yap: gatekeeper for liver size and tumour development. Br J Cancer. 2011; 104:24–32. [PubMed: 21102585]
23. Xu X, Kobayashi S, Qiao W, et al. Induction of intrahepatic cholangiocellular carcinoma by liver-specific disruption of Smad4 and Pten in mice. J Clin Invest. 2006; 116:1843–52. [PubMed: 16767220]
24. Sharpless NE, Depinho RA. The mighty mouse: genetically engineered mouse models in cancer drug development. Nat Rev Drug Discov. 2006; 5:741–54. [PubMed: 16915232]
25. Tuveson D, Hanahan D. Translational medicine: Cancer lessons from mice to humans. Nature. 2011; 471:316–7. [PubMed: 21412332]
26. Jackson EL, Willis N, Mercer K, et al. Analysis of lung tumor initiation and progression using conditional expression of oncogenic K-ras. Genes Dev. 2001; 15:3243–8. [PubMed: 11751630]
27. Jonkers J, Meuwissen R, van der Gulden H, Peterse H, van der Valk M, Berns A. Synergistic tumor suppressor activity of BRCA2 and p53 in a conditional mouse model for breast cancer. Nat Genet. 2001; 29:418–25. [PubMed: 11694875]
28. Postic C, Magnuson MA. DNA excision in liver by an albumin-Cre transgene occurs progressively with age. Genesis. 2000; 26:149–50. [PubMed: 10686614]
29. Duncan AW, Dorrell C, Grompe M. Stem cells and liver regeneration. Gastroenterology. 2009; 137:466–81. [PubMed: 19470389]
30. Komuta M, Spee B, Vander Borght S, et al. Clinicopathological study on cholangiolocellular carcinoma suggesting hepatic progenitor cell origin. Hepatology. 2008; 47:1544–56. [PubMed: 18393293]
31. Jain D, Sarode VR, Abdul-Karim FW, Homer R, Robert ME. Evidence for the neoplastic transformation of Von-Meyenburg complexes. Am J Surg Pathol. 2000; 24:1131–9. [PubMed: 10935654]
32. Tannapfel A, Sommerer F, Benicke M, et al. Genetic and epigenetic alterations of the INK4a-ARF pathway in cholangiocarcinoma. J Pathol. 2002; 197:624–31. [PubMed: 12210082]
33. Taniai M, Higuchi H, Burgart LJ, Gores GJ. p16INK4a promoter mutations are frequent in primary sclerosing cholangitis (PSC) and PSC-associated cholangiocarcinoma. Gastroenterology. 2002; 123:1090–8. [PubMed: 12360471]
34. Sherr CJ. Principles of tumor suppression. Cell. 2004; 116:235–46. [PubMed: 14744434]
35. Engelman JA, Chen L, Tan X, et al. Effective use of PI3K and MEK inhibitors to treat mutant Kras G12D and PIK3CA H1047R murine lung cancers. Nat Med. 2008; 14:1351–6. [PubMed: 19029981]
36. Bekaii-Saab T, Phelps MA, Li X, et al. Multi-institutional phase II study of selumetinib in patients with metastatic biliary cancers. J Clin Oncol. 2011; 29:2357–63. [PubMed: 21519026]
37. McCormick F. Success and failure on the ras pathway. Cancer Biol Ther. 2007; 6:1654–9. [PubMed: 18245956]
38. Yang S, Wang X, Contino G, et al. Pancreatic cancers require autophagy for tumor growth. Genes Dev. 2011; 25:717–29. [PubMed: 21406549]
39. Guo JY, Chen HY, Mathew R, et al. Activated Ras requires autophagy to maintain oxidative metabolism and tumorigenesis. Genes Dev. 2011; 25:460–70. [PubMed: 21317241]
40. Lock R, Roy S, Kenific CM, et al. Autophagy facilitates glycolysis during Ras-mediated oncogenic transformation. Mol Biol Cell. 2011; 22:165–78. [PubMed: 21119005]
41. Kimmelman AC. The dynamic nature of autophagy in cancer. Genes Dev. 2011; 25:1999–2010. [PubMed: 21979913]
42. Klionsky DJ, Abeliovich H, Agostinis P, et al. Guidelines for the use and interpretation of assays for monitoring autophagy in higher eukaryotes. Autophagy. 2008; 4:151–75. [PubMed: 18188003]
43. Jarnagin WR, Weber S, Tickoo SK, et al. Combined hepatocellular and cholangiocarcinoma: demographic, clinical, and prognostic factors. Cancer. 2002; 94:2040–6. [PubMed: 11932907]

NIH-PA Author Manuscript

NIH-PA Author Manuscript

NIH-PA Author Manuscript

44. Woo HG, Lee JH, Yoon JH, et al. Identification of a cholangiocarcinoma-like gene expression trait in hepatocellular carcinoma. Cancer Res. 2011; 70:3034–41. [PubMed: 20395200]

45. Weihrauch M, Benicke M, Lehnert G, Wittekind C, Wrbitzky R, Tannapfel A. Frequent k- ras -2 mutations and p16(INK4A)methylation in hepatocellular carcinomas in workers exposed to vinyl chloride. Br J Cancer. 2001; 84:982–9. [PubMed: 11286481]

46. Bardeesy N, Cheng KH, Berger JH, et al. Smad4 is dispensable for normal pancreas development yet critical in progression and tumor biology of pancreas cancer. Genes Dev. 2006; 20:3130–46. [PubMed: 17114584]

47. Hou YJ, Dong LW, Tan YX, et al. Inhibition of active autophagy induces apoptosis and increases chemosensitivity in cholangiocarcinoma. Lab Invest. 2011; 91:1146–57. [PubMed: 21647092]

48. Dong LW, Hou YJ, Tan YX, et al. Prognostic significance of Beclin 1 in intrahepatic cholangiocellular carcinoma. Autophagy. 2011; 7(10):1222–9. [PubMed: 21654208]

49. Bardeesy N, Aguirre AJ, Chu GC, et al. Both p16(Ink4a) and the p19(Arf)-p53 pathway constrain progression of pancreatic adenocarcinoma in the mouse. Proc Natl Acad Sci U S A. 2006; 103:5947–52. [PubMed: 16585505]

NIH-PA Author Manuscript

NIH-PA Author Manuscript

NIH-PA Author Manuscript

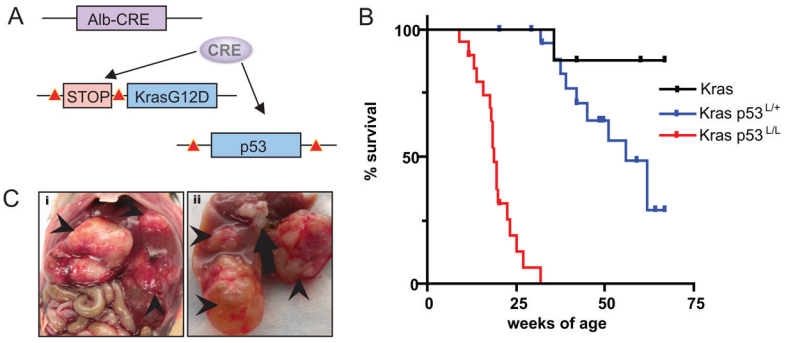

Figure 1.

$Kras^{G12D}$ and p53 mutation in the hepatic epithelium cooperate to cause cholangiocarcinoma. A) Modeling strategy; compound mutant mice harboring albumin-Cre transgene, LSL-$Kras^{G12D}$, and $p53^{L/L}$ were created to conditionally activate $Kras^{G12D}$ and delete p53 in the hepatic epithelium. Lox P sites are indicated with red triangles. B) Kaplan-Meier survival analysis of cohorts of compound mutant animals. The p53 status is indicated; all of the mice have the LSL–$Kras^{G12D}$ allele. C) Gross tumor nodules in the Kras-p53 model. Arrowheads indicate tumor nodules seen in an animal with three distinct tumors. The arrow in image **ii** indicates enlarged lymph nodes. The tumor in the lower aspect of image **ii** is cystic and fluid- filled and was found to be an IPBN.

NIH-PA Author Manuscript
NIH-PA Author Manuscript
NIH-PA Author Manuscript

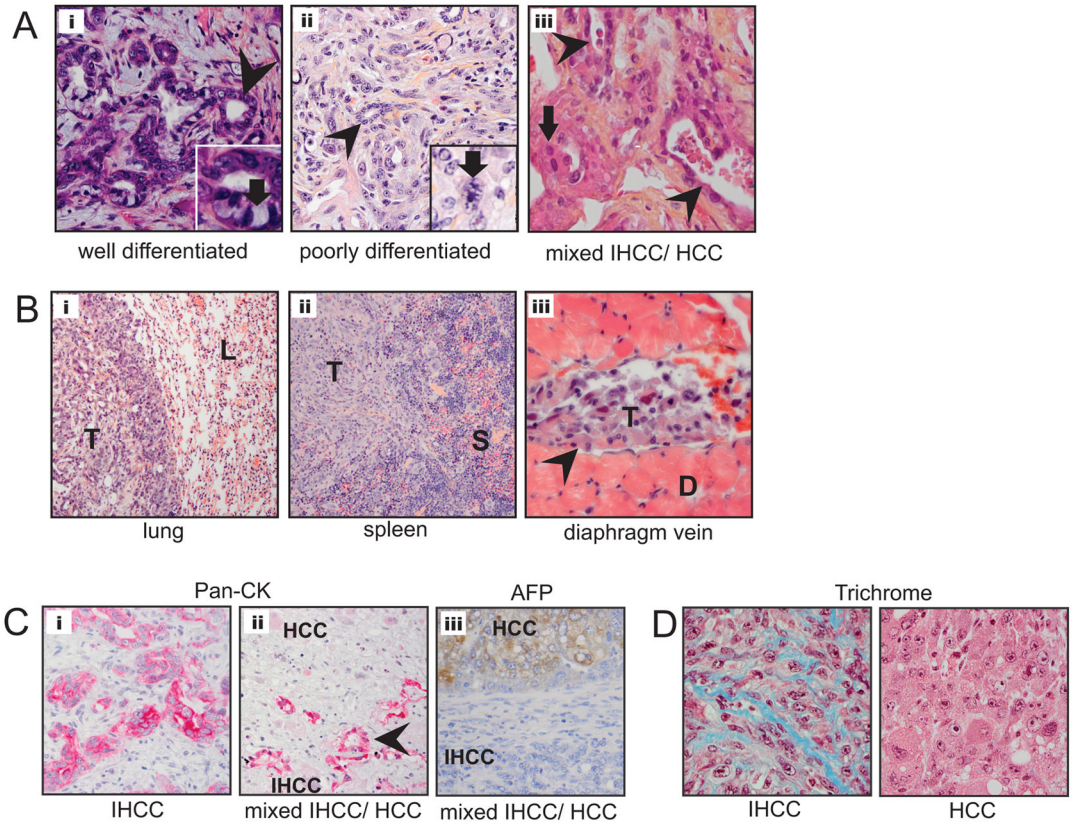

Figure 2.

Kras-p53 IHCC recapitulates the histology of the human disease. A) Histology of primary liver tumors; from left to right i) well-differentiated IHCC 200X with inset demonstrating mucin producing cells (arrow), **ii)** poorly differentiated IHCC 200X with inset demonstrating mitotic figure (arrow) and, **iii)** mixed IHCC/HCC with arrow pointing towards area of HCC vs. glandular appearance of IHCC (arrowhead). B) Extensive metastasis (indicated by letter **T**) were observed grossly and histologically in the **i)** lung (L) **ii)** spleen (S) and **iii)** within the diaphragmatic lymphatic system. C) Pan-cytokeratin IHC of IHCC (i) and mixed IHCC/HCC (ii), upper region is non-staining HCC component and lower region showing glandular structures (arrowhead) which are pan-CK positive. AFP IHC of mixed IHCC/HCC (iii), upper region is AFP staining HCC component and lower region showing non-staining IHCC component. D) Trichrome IHC demonstrating collagen deposition within IHCC (left) but not in HCC (right).

NIH-PA Author Manuscript

NIH-PA Author Manuscript

NIH-PA Author Manuscript

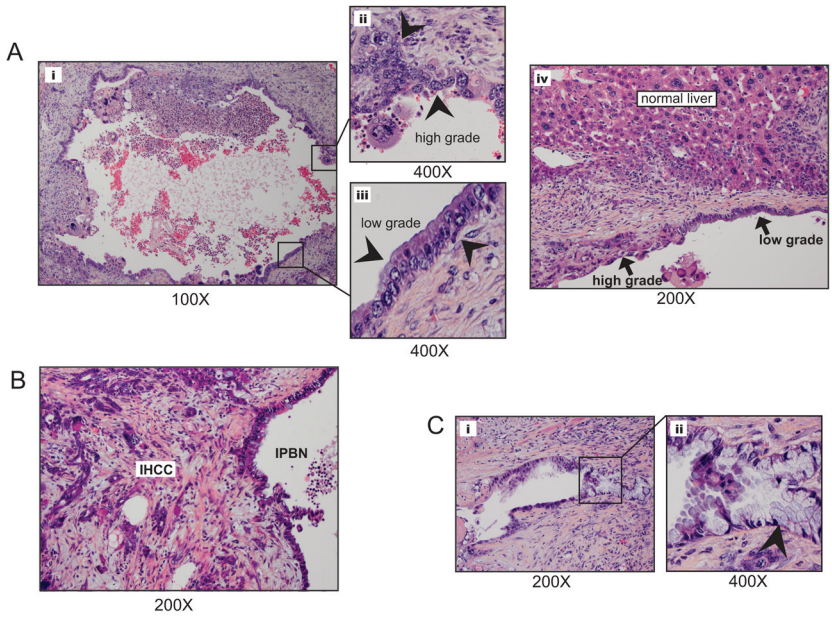

Figure 3.

IPBN is identified separately and in association with IHCC, demonstrating areas of low and high-grade cellular atypia. A) Fluid filled cystic structure (i; low power) demonstrated progressive cellular atypia (ii and iii) arrowheads point to epithelium showing an atypical low grade columnar biliary epithelium (ii) and high grade region with large nuclei, prominent nucleoli and marked cellular atypia (iii). IPBN were found within the context of normal liver (A;iv). B) IPBN adjacent and contiguous with invasive IHCC. C) Smaller IPBN (i) displayed an intestinal type epithelium (ii; arrowhead indicates mucin producing cell).

NIH-PA Author Manuscript

NIH-PA Author Manuscript

NIH-PA Author Manuscript

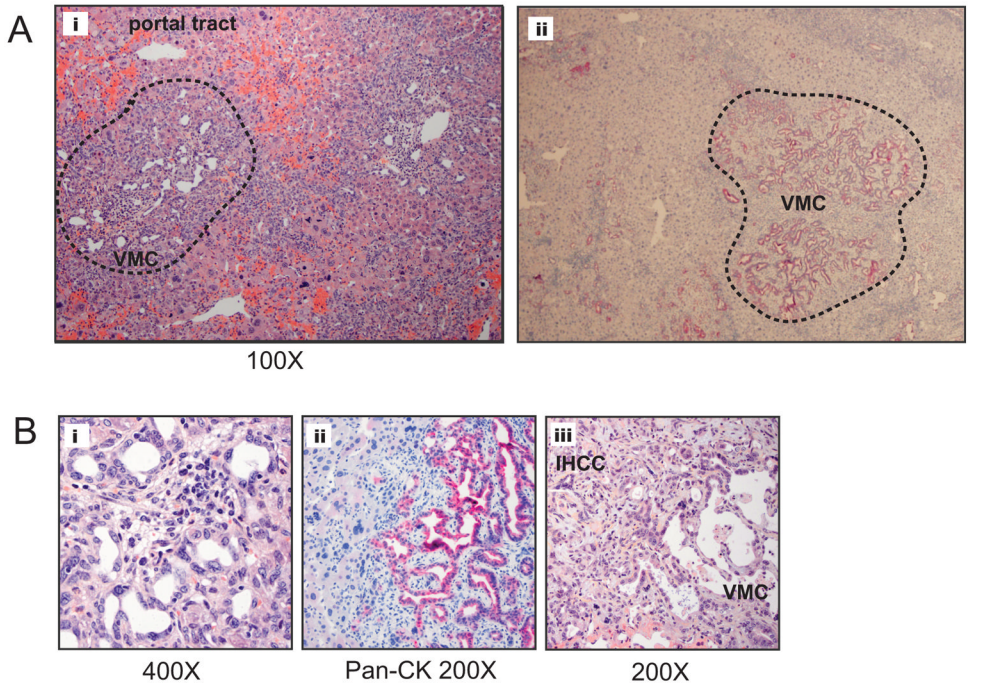

Figure 4.

Von Meyenburg complexes (VCM), or biliary hamartomas, are prevalent and found in association with IHCC in the Kras-p53 model. A) i; Low-power view of Von Meyenburg Complex (circled in dashed black line between portal tracts). ii; IHC with pan-CK Ab of VMC within the hepatic parenchyma. B) i; VMC at high power demonstrated small caliber biliary epithelium surrounded by stroma, ii; VMC demonstrates strong staining with pan-CK Ab, iii; VMC associated with a well differentiated cholangiocarcinoma.

NIH-PA Author Manuscript

NIH-PA Author Manuscript

NIH-PA Author Manuscript

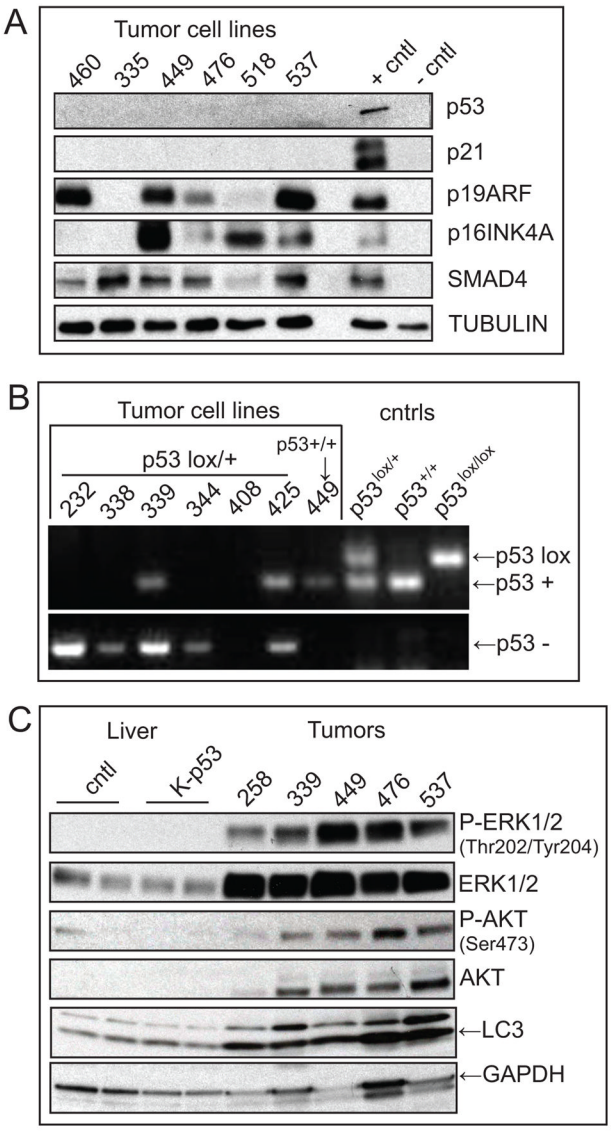

Figure 5.

IHCC harbors molecular derangements characteristic of the human disease and activation of downstream RAS effecter pathways. A) Early passage (P1–3) IHCC cell lysates were tested for the expression of tumor suppressor genes. 25 μg of protein were loaded in each lane and murine pancreatic cell lines with previously defined genetic profiles (p53 or Ink4a/Arf mutant vs. wild-type) were used as controls (49). p53 expression is absent in all IHCC as is p21 expression. While the majority of tumors retained expression of p19Arf line #335 lost expression. Lines #460 and 335 both demonstrated absent p16Ink4a expression. SMAD4 expression was maintained across all lines. B) PCR reactions to detect the p53-WT (+) and p53lox alleles (Upper) and p53-null (−) allele (Lower) in normal tissue (tail clip) from p53lox/lox (lane 10), p53+/+ (lane 9), and p53 lox/+ (lane 8) mice and in tumor cell lines (lanes1–7). Primers and conditions used are previously described in detail (27). 4/6 tumor cell lines from Kras-$p53^{L/+}$ animals (232, 338, 344, & 408) demonstrated no WT allele indicating loss of heterozygosity at the p53 locus. Tumor line 408 demonstrates retention of the p53-null allele with longer exposure (data not shown). Tumor cell line #449 from a Kras-$p53^{+/+}$ animal shows retention of the p53+ allele. C) Western blot analysis of whole

liver lysates from 10 weeks old wild-type and Kras-p53$^{L/L}$ animals compared with IHCC tumor lysates evaluating the relative activity of RAS effecters ERK and AKT demonstrating activity of ERK and AKT. Total LC3 levels were increased in IHCC as compared with normal and mutant liver (LC3 is lower band, upper band is non-specific).

NIH-PA Author Manuscript
NIH-PA Author Manuscript
NIH-PA Author Manuscript

NIH-PA Author Manuscript
NIH-PA Author Manuscript
NIH-PA Author Manuscript

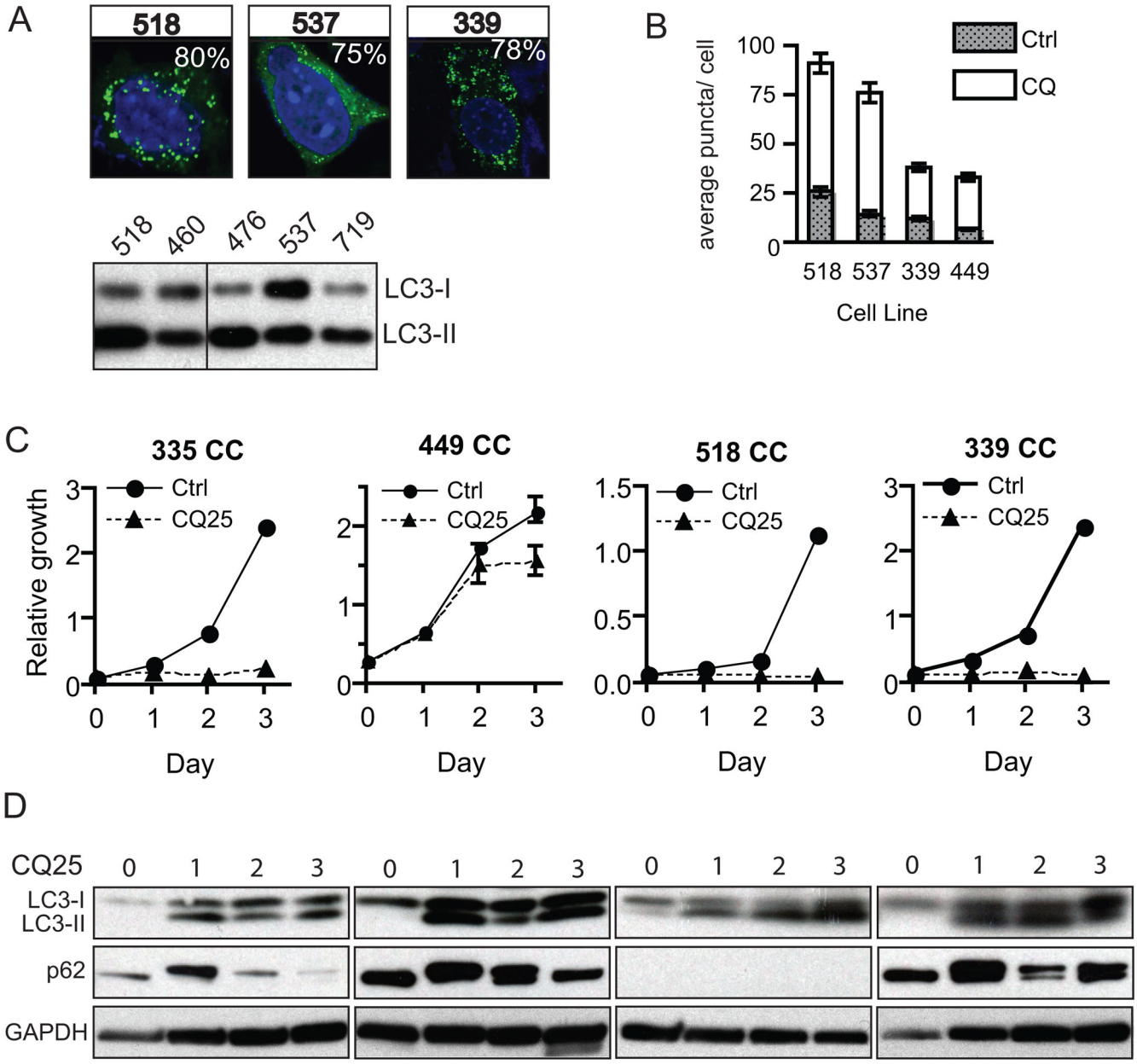

Figure 6.

Kras-p53 IHCC exhibits high basal levels of autophagy and is growth inhibited by chloroquine. A) IHCC cells were infected with a retrovirus expressing GFP-LC3 and grown in complete media with serum and fixed for confocal fluorescence microscopy. These were analyzed for the presence of LC3 dots, representing autophagic vesicles, and quantified. The % of autophagic cells (out of total number of 100 counted) with > 5 foci are shown in the upper right corners of each picture. Below is shown a western blot demonstrating high levels of LC3-II as compared with LC3-I, also consistent with a high level of basal autophagy. B) IHCC cells were cultured under normal growth conditions where the total number of LC3 foci was markedly increased in the presence of CQ (error bars are shown, students t-test is used for comparison, $p < 0.001$ for all cell lines treated). C & D) Growth of IHCC cell lines is inhibited in the presence of CQ $p = <0.001$ for samples 335, 518, and 339 and $p = <0.01$ for

NIH-PA Author Manuscript

NIH-PA Author Manuscript

NIH-PA Author Manuscript

samples 449 (two-way ANOVA, error bars are shown for all data points, those not evident on the graphs fall within the area encompassed by the triangle or circle data-point). Consistent with a block in autophagic flux induced by CQ treatment we observed that treated lines had an accumulation of LC3-II and induction of p62 as compared with Day 0 control, with the exception of #518 where p62 expression was absent.

NIH-PA Author Manuscript
NIH-PA Author Manuscript
NIH-PA Author Manuscript

Cancer Res. Author manuscript; available in PMC 2012 September 15.

Table 1

Tumor histology, # of nodules, precursor lesions found, sites of metastasis, and age.

	ID	Age (wk)	Tumor Type	Size (cm)	Cancer Precursor	Gross metastasis/invasion
$Kras^{G12D}$ $P53^{L/L}$	100	9.0	HCC	1.5	none	None
	460	11.7	Mixed Mixed Mixed	0.5 0.4 1.3	IPBN	Lung, spleen, under liver diaphragm, stomach, pancreas
	199	13.1	CC	1.5	unknown	unknown
	444	15.7	CC	2.0	unknown	Diaphragm, intestine, pancreas, lung
	537	18.1	CC CC	1.0 0.5	VMC	Lung, diaphragm, lymph nodes
	518	18.3	CC	0.4	none	Lymph nodes, stomach
	258	18.4	CC Mixed CC	0.3 0.6 1.3	IPBN	None
	449	18.7	CC	0.5	VMC	Lower lymph nodes
	254	19.4	HCC	3.0	unknown	None
	335	19.6	CC	1.0	VMC	Lymph nodes, intestine
	520	19.9	CC	0.5	VMC	Diaphragm
	257	23.3	HCC CC	1.0 0.3	none	Lung
	476	32.0	CC	0.5	none	Lungs, lymph nodes
	719	17.6	CC CC CC	1.0 2.0 2.0	IPBN	Lung, diaphragm, lymph nodes

NIH-PA Author Manuscript

NIH-PA Author Manuscript

NIH-PA Author Manuscript

	ID	Age (wk)	Tumor Type	Size (cm)	Cancer Precursor	Gross metastasis/invasion
$Kras^{G12D}$ $P53^{L/+}$	232	31.9	HCC	2.0	none	None
	339	37.6	CC Mixed	2.0 2.5	none	Lung
	231	39.1	CC	1.0	none	Intestine, pancreas
	421	41.9	HCC	0.3	none	None
	425	45.1	CC	2.0	VMC	Lungs, pancreas, lymph nodes, stomach
	338	51.0	HCC	1.0	none	None
	344	61.7	CC	2.2	IPBN	Lungs, lymph nodes
	408	61.7	CC	1.6	none	Lungs, lymph nodes, intestine
$Kras^{G12D}$	495	35.7	CC	2.0	unknown	None